ACS Photonics

Article

Cite This: ACS Photonics 2018, 5, 4164–4169

pubs.acs.org/journal/apchd5

Radiation-Pressure-Antidamping Enhanced Optomechanical Spring Sensing

Fei Pan, Kaiyu Cui,* Guoren Bai, Xue Feng, Fang Liu, Wei Zhang, and Yidong Huang

Department of Electronic Engineering, Beijing National Research Center for Information Science and Technology (BNRist), Tsinghua University, Beijing 100084, China

Supporting Information

ABSTRACT: On-chip refractive index sensing plays an important role in many fields, ranging from chemical, biomedical, and medical to environmental applications. Recently, optomechanical cavities have emerged as promising tools for precision sensing. In view of the sensors based on optomechanical cavities, the Q factor of mechanical modes is a key parameter for achieving high sensitivity and resolution. Here we demonstrated an integrated optomechanical cavity based on a silicon nanobeam structure. Our cavity supports a fundamental mechanical mode with a frequency of 4.36 GHz and a record-high mechanical Q of 18300 in the ambient environment, facilitated by the radiation-pressure antidamping. The distinctive nature of the optomechanical spring sensing approach combined with our high mechanical Q silicon cavity allows for a sensing resolution of $\delta\lambda/\lambda_0 \sim 10^{-7}$, which is at least 1 order of magnitude higher than that of conventional silicon-based approaches and paves the way for on-chip sensors with unprecedented sensitivity.

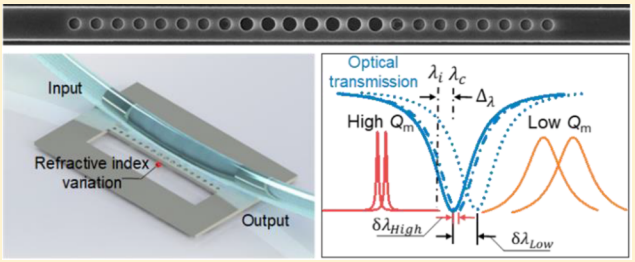

KEYWORDS: *optomechanical crystal, silicon nanobeam, optomechanical cavity, optical spring effect, radiation-pressure antidamping, refractive index sensing, precision sensing, mechanical quality factor*

On-chip ultimate-precision refractive index sensing benefits many applications ranging from chemical measurements, biomedical analysis, and medical diagnostics to environmental monitoring.[1,2] Among a variety of sensing approaches, a high-Q optical microcavity is a prime candidate for on-chip sensing due to its advantages of high sensitivity and label-free detection.[3] Since its sensing mechanism relies on either reactive interaction (i.e., dispersion) by detecting the resonance shift or dissipative interaction by detecting the change in line width, the sensing resolution depends critically on the optical Q.[4] To improve sensing accuracy, researchers have made great efforts to achieve high-Q optical cavities.[5−7] For example, dielectric materials (glass, silicon nitride, and various hybrid materials) are routinely chosen to reduce intrinsic loss and acquire high optical Q (>10^8) with ultrasmooth microspheres and microtoroids formed under surface tension.[8−10] However, such high-Q optical cavities are difficult to integrate with other units of devices, let alone compatible with COMS fabrication. On the other hand, silicon-based resonators are expected to be more promising sensing candidates due to their higher refractive index, well-established capability for fabrication of nanostructures, well-developed multifunctional integrated devices, and relatively high optical Q.[11,12] However, until now, the highest optical Q reported for a silicon-based microcavity[13] is about 10^6, yielding a resolution of $\delta\lambda/\lambda_0 \sim 10^{-6}$ for index sensing[2] and, thus, severely hindering further improvement of the silicon-based on-chip ultimate-precision sensing.[2]

In recent years, optomechanical cavities have been regarded as promising platforms for precision sensing,[14−17] which have been put forward to detect the movement of mechanical oscillators with light. In such a system, a high mechanical Q is crucial for improving the sensitivity because the sensing principle underlies the detection of the mechanical mode shift.[18] However, the mechanical mode is remarkably damped in the ambient environment owing to the internal damping and, also, the inevitable coupling between the mechanical system and the atmosphere at room temperature.[19] Certain efforts have been made to effectively reduce the damping loss from mechanical vibration and consequently to improve the mechanical Q by using vacuum or cryogenic measurements.[14,20] Nevertheless, vacuum or cryogenic conditions give rise to severe technical challenges and fundamental constraints for practical applications.[2,21] Most recently, researchers demonstrated a coherent optomechanical oscillation of a silica microsphere with an ultrahigh quality factor in aqueous environment for the first time,[22] and using the optical spring effect to dramatically enhance the sensing resolution by approximately a factor of mechanical Q compared with previous approaches.[17] Despite these advances, however, optomechanical index sensing in silicon has not yet been reported, which can be expected to enable high-sensing

Received: July 16, 2018
Published: September 6, 2018

DOI: 10.1021/acsphotonics.8b00968
ACS Photonics 2018, 5, 4164–4169

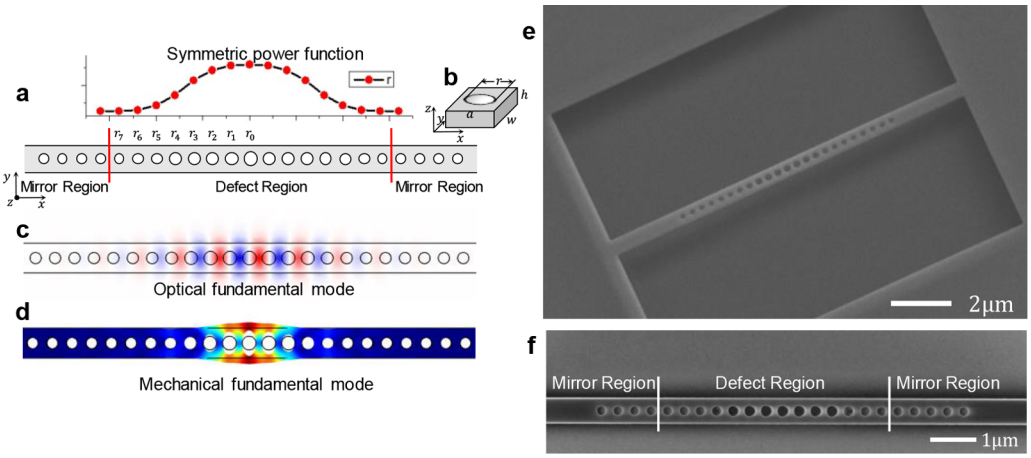

Figure 1. Cavity structure and simulated field profiles. (a) Plan-view schematic of the nanobeam optomechanical cavity, where the radii r_n of the defect unit cells are transformed as the symmetric power function of eq 1 and vary from r_0 (127.9 nm) to r_7 (105.3 nm; red curve). (b) Unit cell with parameters (a, w, h) = (364.8 nm, 556 nm, 220 nm), which are used to describe the nanobeam in both the defect and mirror regions. (c) Normalized electric y-component of the localized optical fundamental mode. (d) Normalized displacement field of the confined fundamental mechanical mode with frequency of 4.38 GHz. (e) Scanning electron microscope (SEM) image with an oblique view of the fabricated nanobeam cavity. (f) SEM image with a top view of the cavity.

precisions and integrated capabilities with other multifunctional on-chip devices.

In this work, aiming to develop on-chip precision sensing, we demonstrate a high mechanical Q silicon nanobeam optomechanical cavity via radiation-pressure antidamping. The proposed microcavity is designed based on optomechanical crystals (OMCs), with the hole radius of the cavity defect region following a symmetric power (SP) function to reduce the optical radiation loss, namely, SP-OMC cavity. The measured intrinsic optical Q can reach 3.8×10^4, yielding a strong radiation pressure in the cavity. Thus, both an optical spring effect and reduced mechanical damping rate are observed, which improve the sensing accuracy. The measured mechanical frequency of the fundamental mechanical mode of the cavity is 4.36 GHz, and the mechanical Q can reach 18300 in the ambient environment assisted by the radiation pressure, which, to the best of our knowledge, is a record-high mechanical Q in the ambient environment. This approach based on the use of a high mechanical Q optomechanical cavity enables a sensing resolution of $\delta\lambda/\lambda_0 \sim 10^{-7}$, which is at least 1 order of magnitude higher than that of conventional silicon-based optical approaches.[13] Compared to the previous reports,[23,24] which possess a sensing resolution of $\delta\lambda/\lambda_0 \sim 1.2 \times 10^{-5}$, and have demonstrated the detection of single polystyrene nanoparticles with radius of 12.5 nm and single streptavidin molecule, our work with sensing resolution of $\delta\lambda/\lambda_0 \sim 10^{-7}$ has great potential for the detection of single nanoparticles or even single molecules, and sheds light on on-chip sensing components with unprecedented precision.

RESULTS AND DISCUSSION

Structural Design and Fabrication. A schematic of the proposed nanobeam SP-OMC cavity is shown in Figure 1a, where a defect region in the center is sandwiched between two identical periodic mirror regions. A unit cell of the proposed structure with a uniform width (w) of 556 nm and a height (h) of 220 nm is shown in Figure 1b. The OMC pitches (a) are set to 364.8 nm for both the defect region and the two mirror regions. For the defect region shown in the inset of Figure 1a, the hole radius changes from r_0 (127.9 nm) to r_7 (105.3 nm), following a SP function given in eq 1. The periodic regions can form both an optical and mechanical bandgap to simultaneously confine the defect optical and mechanical modes in the SP-OMC cavity (see Supporting Information for details). Here, the SP function is chosen for a smoother evolution than linear transition, since it is intuitively plausible that the transition between the adjacent regions is much smaller, thus reducing the scattering loss to achieve high optical Q. As expected, the designed optical Q can reach 50000, which is beneficial to enhancing the radiation pressure[25] and ultimately enhancing the sensing precision.

$$r_n = \begin{cases} r_0 - \dfrac{(r_0 - r_7)}{2} \times \left(\dfrac{n}{3.5}\right)^{3.2}, & n = 0, 1, 2, 3 \\ r_7 + \dfrac{(r_0 - r_7)}{2} \times \left(\dfrac{7 - n}{3.5}\right)^{3.2}, & n = 4, 5, 6, 7 \end{cases} \quad (1)$$

The simulated field profiles for our design are shown in Figure 1c,d, corresponding to the normalized electric y-component of the localized optical fundamental mode and the normalized displacement field of the confined fundamental mechanical mode, respectively. Due to the optical mode and the mechanical mode being simultaneously well confined in our structure, a high optomechanical coupling rate of 820 kHz is obtained, which eventually results in the observed radiation-pressure induced optical spring effect and amplification process.

The designed structure is fabricated on a silicon-on-insulator (SOI) wafer with a 220 nm thick device layer and a 3 μm buried oxide layer. Figure 1e,f shows the scanning electron microscope (SEM) images of the fabricated nanobeam cavity. For fabrication, the cavity pattern is first defined by electron beam lithography (EBL), and then transferred to the silicon layer by inductively coupled plasma (ICP) etching. Finally, the suspended nanobeam is released by wet etching using buffered hydrofluoric acid (HF) solution to remove the buried oxide layer beneath the nanobeam. The fabricated structure keeps the same geometric parameters as designed.

DOI: 10.1021/acsphotonics.8b00968
ACS Photonics 2018, 5, 4164−4169

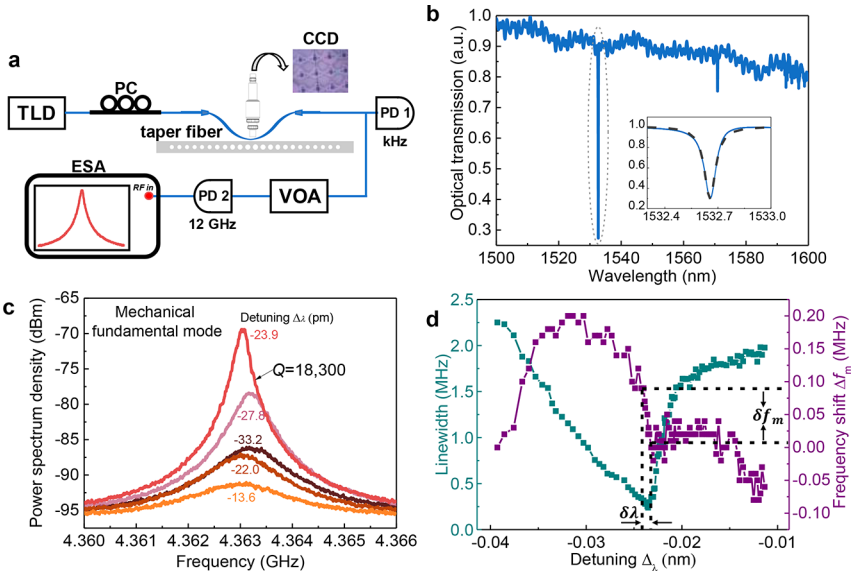

Figure 2. Experimental schematics and measurement results. (a) Experimental setup: TLD, tunable laser diode; PC, polarization controller; PD1, photodetector with a bandwidth of approximately a kilohertz; PD2, photodetector with a bandwidth of 12 GHz; VOA, viable optical attenuator; ESA, electrical spectrum analyzer. (b) Optical transmission spectrum showing two dips, which correspond to two optical resonances, centered at 1532.65 and 1570.88 nm, respectively. The inset shows a Lorentzian fitting of the fundamental optical mode. (c) Series of power spectrum densities (PSDs) for the fundamental mechanical mode referred to as different laser detuning (Δ_λ, denotes the detuning between the input laser λ_i and the cavity resonance λ_c, that is, $\Delta_\lambda = \lambda_i - \lambda_c$) from −33.2, −27.8, −23.9, and −22.0 to −13.6 pm, respectively. (d) Evolution of the measured mechanical resonant frequency (purple) and the corresponding mechanical line width (dark green) under different Δ_λ.

Measurements. The performance of the proposed SP-OMC cavity is characterized using the experimental setup shown in Figure 2a. Here, we choose the fiber-optical characterization setup in the ambient environment,[26] as detailed in Methods. Taking into account the difference of the refraction index between the silica fiber and the silicon nanobeam, the coupling efficiency can be further improved with a new way reported in ref 27. The optical transmission spectrum is presented in Figure 2b, which reveals the characteristic of the optical cavity. The fundamental optical mode (λ = 1532.65 nm) and the first-order optical mode (λ = 1570.88 nm) are observed in the transmission spectrum. Based on Lorentzian fitting to the fundamental optical mode, shown in the inset of Figure 2b, the measured total optical Q and the intrinsic optical Q for the fundamental optical mode can be inferred to be 2×10^4 and 3.8×10^4, respectively. The lower optical Q than that of the simulation result is primarily caused by inevitable scattering loss due to fabrication imperfections (see Supporting Information for more details).

With a high optical Q, the laser light inside the cavity gives rise to a strong radiation pressure,[25] and the results are very interesting. Distinctive dynamical effects in an optomechanical cavity arise from the retarded nature of the radiation pressure. More specifically, the optical gradient force created by radiation pressure will change with laser-cavity detuning (Δ_λ, defined as the difference between the input laser λ_i and cavity resonance λ_c, i.e., $\Delta_\lambda = \lambda_i - \lambda_c$), which means that the effective rigidity and the effective mechanical loss rate are modified.[28,29] The former manifests an optical spring effect, and the latter results in a change in the full effective mechanical damping rate[19,30] (see Supporting Information for details).

To experimentally observe the effects resulting from the radiation pressure, the input light (λ_i) is first set away from the cavity resonance (λ_c) and then gradually set closer to λ_c. In our work, the input light is blue detuned during the whole procedure, or in other words, Δ_λ is negative all the time. The blue-detuned input laser will lead to an amplification and heating of the vibration modes,[25] and thus, we can obtain a dramatically high mechanical Q. Figure 2c shows the sequence of power spectrum densities (PSDs) for the fundamental mechanical mode, and the data show that both the frequency and the line width of the mechanical resonance change with the detuning. The evolution of the mechanical frequency and the line width with various detuning values is presented in Figure 2d. Evidently, when the input laser is far away from the cavity resonance, the optically induced dynamical backaction is sufficiently small, and the measured mechanical mode and the thermal Brownian vibration are not very different. As laser input gradually approaches λ_c, the dynamical effects will be more influenced since the radiation pressure becomes increasingly stronger, leading to two consequences. On the one hand, the measured mechanical frequency shifts with Δ_λ, which indicates a modified effective rigidity attributed to the optical spring effect. On the other hand, the mechanical line width is adjusted because the optical gradient force originating from the radiation pressure will cause antidamping in the blue-detuned ($\Delta_\lambda < 0$) regime, consequently leading to an amplification of thermal fluctuations. Obviously, the effective mechanical line width is dramatically reduced, corresponding to a measured mechanical Q as high as 18300, even in the ambient environment. It should be noted that the antidamping enhanced mechanical Q is obtained before the coherent and regenerative optomechanical oscillation (see Supporting Information for details). Since the frequency and line width of a mechanical mode is sensitive to laser-cavity detuning, we can use it to realize high-precision refractive index sensing, whereas a variation in the refractive index will alter the cavity resonance, thus, changing the detuning.

Refractive Index Sensing. In the following discussion, we provide a scenario to demonstrate the sensing principle of the

DOI: 10.1021/acsphotonics.8b00968
ACS Photonics 2018, 5, 4164−4169

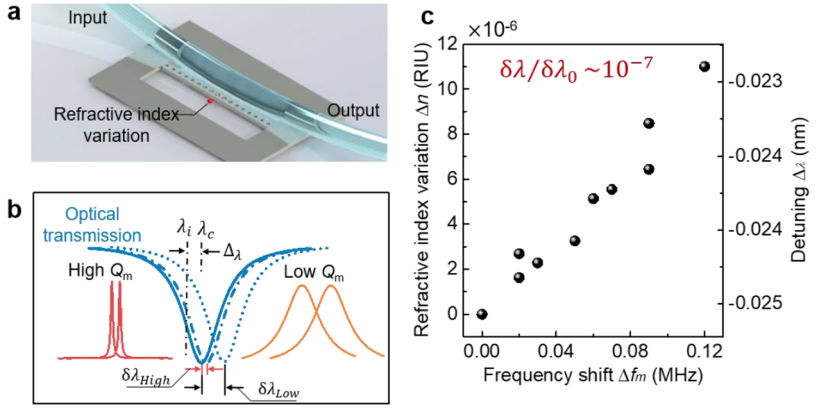

Figure 3. Refractive index sensing based on an optomechanical cavity. (a) Refractive index variation (Δn) in the surroundings of the cavity where a particle appears. (b) Refractive index sensing mechanisms for the mechanical modes with different mechanical Q values. $\delta\lambda_{high}$ and $\delta\lambda_{low}$ are the different wavelength shifts in the optical cavity, corresponding to different minimum detectable Δf_m caused by a high or low mechanical Q. (c) Refractive index variation and the corresponding detuning Δ_λ vs the frequency shift Δf_m.

optomechanical cavity and how resolution is improved. When the refractive index (Δn) varies slightly in the surroundings of the cavity, such as a particle appearing near to the SP-OMC cavity, as shown in Figure 3a, the cavity resonance will shift and cause detuning (Δ_λ) between the fixed input laser and cavity resonance. The discussion below is based on that the particle can be trapped at a fixed position via the optical gradient force.[31,32] Considering the mechanical mode's sensitivity to laser-cavity detuning (caused by Δn), we can distinguish the index variation by measuring the mechanical frequency shift Δf_m, as shown in Figure 3b, instead of the shift in the optical mode as in conventional methods (see Supporting Information for details). The advantage is that the sensing resolution can be improved dramatically, because in an amplification and heating process, the mechanical line width can be strikingly narrowed with the assistance of the restoring radiation pressure (Figure 3b). Therefore, the extremely small detectable Δf_m determined by the high mechanical Q refers to a much smaller wavelength shift in the optical cavity ($\delta\lambda_{high}$), as presented in Figure 3b. In other words, the detectable limit for index sensing (Δn) is dramatically reduced by the high mechanical Q via the radiation-pressure antidamping. To further understand the sensing ability,[33] the refractive index variations can be predicted from experimental data as shown Figure 3c. Here, we did not do the real sensing experiment by delivering the particles to the nanobeam. The sensing resolution is evaluated from the experimental data of optical spring effect as follows. The input laser is initially set at a laser-cavity detuning of $\Delta_\lambda = -0.0232$ nm for a suitable operating regime of sensing. The specified detuning ensures a high mechanical Q together with a large optical frequency change with a tuning slope of df_m/Δ_λ due to magnification of the optical spring effect. Based on our experiments, the obtained mechanical Q of 18300 is capable of reducing the minimum detectable Δf_m from 2.4 MHz to 240 kHz in our device. Meanwhile, the optical spring effect amplifies the change in the optical frequency with a tuning slope of $df_m/\Delta_\lambda \sim -0.2$ GHz/nm, as inferred from the data in Figure 2d. Thus, by incorporating the merits of high mechanical Q and an amplified change of the optical resonance, the final sensing resolution can reach $\delta\lambda/\lambda_0 \sim 10^{-7}$ (see Supporting Information for details), which is at least 1 order of magnitude higher than that of the conventional silicon-based optical approaches.

CONCLUSION

In summary, we demonstrate a nanobeam SP-OMC cavity in which the gradient air-holes are designed using a symmetric power function, and analyze the precision sensing ability arising from high mechanical Q via the radiation-pressure antidamping. The measured SP-OMC cavity supports a fundamental optical mode and mechanical mode with frequencies of 195.74 THz and 4.36 GHz, respectively. The intrinsic optical Q can reach 3.8×10^4 in experiments, yielding a strong radiation pressure in the OMC cavity. Thus, an optical spring effect and reduced mechanical damping rate under different laser detuning are observed. The former results in a frequency that is sensitively dependent on the optical resonance shift. The latter generates a record-high mechanical Q of 18300 in the ambient environment, which dramatically reduces the minimum detectable mechanical resonance shift compared to its intrinsic vibration. Due to these two effects brought about by the radiation-pressure antidamping, an ultimate sensing resolution as high as $\delta\lambda/\lambda_0 \sim 10^{-7}$ is realized, with a higher resolution enhanced by at least two orders predict for low-loss nanofabrication.[13] Therefore, our silicon SP-OMC structure combined with the unique optomechanical spring sensing approach shows admirable promise for broad on-chip index sensing applications.

METHODS

Experimental Setup. We chose a fiber-optical characterization setup in the ambient environment. To ensure an efficient coupling from the taper fiber to the cavity, the light from a tunable laser diode (TLD) is first adjusted to transverse electric (TE) mode with a polarization controller, and then, the output polarized light is delivered to the SP-OMC cavity by an evanescent fiber-optical coupling. The light escaping from the structure is coupled back into the same fiber and separated into two parts by a 10/90 fiber coupler. A small portion, approximately 10% of the laser signal, is fed into a kHz photodetector (PD) to measure the optical properties by sweeping the wavelengths of the TLD. In addition, 90% of the laser signal is sent to a variable optical attenuator (VOA), which is used to ensure a suitable final laser power delivered to the photodetector with a bandwidth of 12 GHz. To measure the mechanical properties of the SP-OMC cavity, the wavelength of the input light must be set near the resonant

DOI: 10.1021/acsphotonics.8b00968
ACS Photonics 2018, 5, 4164−4169

wavelength, followed by an electrical spectrum analyzer (ESA) to monitor the radio frequency response of the mechanical cavity. Note that all measurements were performed in the ambient environment.

■ ASSOCIATED CONTENT

Supporting Information

The Supporting Information is available free of charge on the ACS Publications website at DOI: 10.1021/acsphotonics.8b00968.

Optical and mechanical band structure diagrams, the dynamical backaction due to the retarded nature of the radiation pressure in an optomechanical system, the optomechanical sensing approach for refractive index sensing, analysis of scattering loss due to Rayleigh in nature, and the radiation-pressure-antidamping enhanced mechanical Q (PDF).

■ AUTHOR INFORMATION

Corresponding Author

*E-mail: kaiyucui@tsinghua.edu.cn.

ORCID

Fei Pan: 0000-0001-8883-9246

Xue Feng: 0000-0002-9057-1549

Author Contributions

K.C. and F.P. conceived the study. F.P. performed the theoretical analysis. F.P. and G.B. conducted the experiments. K.C. and F.P. wrote the paper. X.F., F.L., W.Z., and Y.H. discussed the results and reviewed the manuscript.

Funding

This work was supported by the National Key R&D Program of China under Contract No. 2017 YFA0303700, the National Natural Science Foundation of China (Grant Nos. 61775115, 91750206, 61575102, and 61621064), and the Opened Fund of the State Key Laboratory on Integrated Optoelectronics (No. IOSKL2016KF01).

Notes

The authors declare no competing financial interest.

■ ACKNOWLEDGMENTS

We thank Dr. Fengliang Dong in China National Center for Nanoscience and Technology for help with device fabrication.

■ REFERENCES

(1) Shen, Y.; Zhou, J.; Liu, T.; Tao, Y.; Jiang, R.; Liu, M.; Xiao, G.; Zhu, J.; Zhou, Z.-K.; Wang, X.; Jin, C.; Wang, J. Plasmonic Gold Mushroom Arrays with Refractive Index Sensing Figures of Merit Approaching the Theoretical Limit. *Nat. Commun.* **2013**, *4*, 2381.

(2) Fan, X.; White, I. M.; Shopova, S. I.; Zhu, H.; Suter, J. D.; Sun, Y. Sensitive Optical Biosensors for Unlabeled Targets: A Review. *Anal. Chim. Acta* **2008**, *620*, 8−26.

(3) Luchansky, M. S.; Bailey, R. C. High-Q Optical Sensors for Chemical and Biological Analysis. *Anal. Chem.* **2012**, *84*, 793−821.

(4) Shen, B.-Q.; Yu, X.-C.; Zhi, Y.; Wang, L.; Kim, D.; Gong, Q.; Xiao, Y.-F. Detection of Single Nanoparticles Using the Dissipative Interaction in a High- Q Microcavity. *Phys. Rev. Appl.* **2016**, *5*, 024011.

(5) Chen, W. J.; Özdemir, Ş. K.; Zhao, G. M.; Wiersig, J.; Yang, L. Exceptional Points Enhance Sensing in an Optical Microcavity. *Nature* **2017**, *548*, 192−196.

(6) Lu, T.; Lee, H.; Chen, T.; Herchak, S.; Kim, J. H.; Fraser, S. E.; Flagan, R. C.; Vahala, K. High Sensitivity Nanoparticle Detection Using Optical Microcavities. *Proc. Natl. Acad. Sci. U. S. A.* **2011**, *108*, 5976−5979.

(7) He, L.; Özdemir, Ş. K.; Zhu, J.; Kim, W.; Yang, L. Detecting Single Viruses and Nanoparticles Using Whispering Gallery Microlasers. *Nat. Nanotechnol.* **2011**, *6*, 428−432.

(8) Ren, H. C.; Vollmer, F.; Arnold, S.; Libchaber, A. High-Q Microsphere Biosensor - Analysis for Adsorption of Rodlike Bacteria. *Opt. Express* **2007**, *15*, 17410−17423.

(9) Santiago-Cordoba, M. A.; Cetinkaya, M.; Boriskina, S. V.; Vollmer, F.; Demirel, M. C. Ultrasensitive Detection of a Protein by Optical Trapping in a Photonic-Plasmonic Microcavity. *J. Biophotonics* **2012**, *5*, 629−638.

(10) Roy, S.; Prasad, M. Design of All-Optical Reconfigurable Logic Unit with Bacteriorhodopsin Protein Coated Microcavity Switches. *IEEE Transactions on Nanobioscience* **2011**, *10*, 160−171.

(11) Burg, T. P.; Godin, M.; Knudsen, S. M.; Shen, W.; Carlson, G.; Foster, J. S.; Babcock, K.; Manalis, S. R. Weighing of Biomolecules, Single Cells and Single Nanoparticles in Fluid. *Nature* **2007**, *446*, 1066−1069.

(12) Stevens, M. M.; Maire, C. L.; Chou, N.; Murakami, M. A.; Knoff, D. S.; Kikuchi, Y.; Kimmerling, R. J.; Liu, H. Y.; Haidar, S.; Calistri, N. L.; Cermak, N.; Olcum, S.; Cordero, N. A.; Idbaih, A.; Wen, P. Y.; Weinstock, D. M.; Ligon, K. L.; Manalis, S. R. Drug Sensitivity of Single Cancer Cells Is Predicted by Changes in Mass Accumulation Rate. *Nat. Biotechnol.* **2016**, *34*, 1161−1167.

(13) Heylman, K. D.; Knapper, K. A.; Horak, E. H.; Rea, M. T.; Vanga, S. K.; Goldsmith, R. H. Optical Microresonators for Sensing and Transduction: A Materials Perspective. *Adv. Mater.* **2017**, *29*, 1700037.

(14) Krause, A. G.; Winger, M.; Blasius, T. D.; Lin, Q.; Painter, O. A High-Resolution Microchip Optomechanical Accelerometer. *Nat. Photonics* **2012**, *6*, 768−772.

(15) Gil Santos, E.; Baker, C.; Nguyen, D. T.; Hease, W.; Gomez, C.; Lemaître, A.; Ducci, S.; Leo, G.; Favero, I. High-Frequency Nano-Optomechanical Disk Resonators in Liquids. *Nat. Nanotechnol.* **2015**, *10*, 810−816.

(16) Gavartin, E.; Verlot, P.; Kippenberg, T. J. A Hybrid on-Chip Optomechanical Transducer for Ultrasensitive Force Measurements. *Nat. Nanotechnol.* **2012**, *7*, 509−514.

(17) Yu, W.; Jiang, W. C.; Lin, Q.; Lu, T. Cavity Optomechanical Spring Sensing of Single Molecules. *Nat. Commun.* **2016**, *7*, 12311.

(18) Han, K.; Kim, J.; Bahl, G. High-Throughput Sensing of Freely Flowing Particles with Optomechanofluidics. *Optica* **2016**, *3*, 585−591.

(19) Burek, M. J.; Cohen, J. D.; Meenehan, S. M.; El-Sawah, N.; Chia, C.; Ruelle, T.; Meesala, S.; Rochman, J.; Atikian, H. A.; Markham, M.; Twitchen, D. J.; Lukin, M. D.; Painter, O.; Lončar, M. Diamond Optomechanical Crystals. *Optica* **2016**, *3*, 1404−1411.

(20) Chan, J.; Alegre, T. P. M.; Safavi-Naeini, A. H.; Hill, J. T.; Krause, A.; Gröblacher, S.; Aspelmeyer, M.; Painter, O. Laser Cooling of a Nanomechanical Oscillator into Its Quantum Ground State. *Nature* **2011**, *478*, 89−92.

(21) Eom, K.; Park, H. S.; Yoon, D. S.; Kwon, T. Nanomechanical Resonators and Their Applications in Biological/chemical Detection: Nanomechanics Principles. *Phys. Rep.* **2011**, *503*, 115−163.

(22) Yu, W.; Jiang, W. C.; Lin, Q.; Lu, T. Coherent Optomechanical Oscillation of a Silica Microsphere in an Aqueous Environment. *Opt. Express* **2014**, *22*, 21421.

(23) Zhi, Y. Y.; Yu, X. C.; Gong, Q. H.; Yang, L.; Xiao, Y. F. Single Nanoparticle Detection Using Optical Microcavities. *Adv. Mater.* **2017**, *29*, 1604920.

(24) Quan, Q.; Floyd, D. L.; Burgess, I. B.; Deotare, P. B.; Frank, I. W.; Tang, S. K. Y.; Ilic, R.; Lončar, M. Single Particle Detection in CMOS Compatible Photonic Crystal Nanobeam Cavities. *Opt. Express* **2013**, *21*, 32225−32233.

(25) Aspelmeyer, M.; Kippenberg, T. J.; Marquardt, F. Cavity Optomechanics. *Rev. Mod. Phys.* **2014**, *86*, 1391−1452.

(26) Gomis-Bresco, J.; Navarro-Urrios, D.; Oudich, M.; El-Jallal, S.; Griol, A.; Puerto, D.; Chavez, E.; Pennec, Y.; Djafari-Rouhani, B.;

DOI: 10.1021/acsphotonics.8b00968
ACS Photonics 2018, 5, 4164−4169

Alzina, F.; Martínez, A.; Sotomayor Torres, C. A One-Dimensional Optomechanical Crystal with a Complete Phononic Band Gap. *Nat. Commun.* **2014**, *5*, 4452.
(27) Jiang, X. F.; Shao, L. B.; Zhang, S. X.; Yi, X.; Wiersig, J.; Wang, L.; Gong, Q. H.; Lončar, M.; Yang, L.; Xiao, Y. F. Chaos-Assisted Broadband Momentum Transformation in Optical Microresonators. *Science* **2017**, *358*, 344−347.
(28) Sheard, B. S.; Gray, M. B.; Mow-Lowry, C. M.; McClelland, D. E.; Whitcomb, S. E. Observation and Characterization of an Optical Spring. *Phys. Rev. A: At., Mol., Opt. Phys.* **2004**, *69*, 051801.
(29) Mow-Lowry, C. M.; Mullavey, A. J.; Goßler, S.; Gray, M. B.; McClelland, D. E. Cooling of a Gram-Scale Cantilever Flexure to 70 mK with a Servo-Modified Optical Spring. *Phys. Rev. Lett.* **2008**, *100*, 010801.
(30) Paraïso, T. K.; Kalaee, M.; Zang, L.; Pfeifer, H.; Marquardt, F.; Painter, O. Position-Squared Coupling in a Tunable Photonic Crystal Optomechanical Cavity. *Phys. Rev. X* **2015**, *5*, 041024.
(31) Mandal, S.; Serey, X.; Erickson, D. Nanomanipulation Using Silicon Photonic Crystal Resonators. *Nano Lett.* **2010**, *10*, 99−104.
(32) Han, S.; Shi, Y. Systematic Analysis of Optical Gradient Force in Photonic Crystal Nanobeam Cavities. *Opt. Express* **2016**, *24*, 452−458.
(33) Hodaei, H.; Hassan, A. U.; Wittek, S.; Garcia-Gracia, H.; El-Ganainy, R.; Christodoulides, D. N.; Khajavikhan, M. Enhanced Sensitivity at Higher-Order Exceptional Points. *Nature* **2017**, *548*, 187−191.

DOI: 10.1021/acsphotonics.8b00968
ACS Photonics 2018, 5, 4164−4169